Applied Physics B (2023) 129:80
https://doi.org/10.1007/s00340-023-08022-x

Applied Physics B
Lasers and Optics

RESEARCH

Measurement of $\delta^{18}O$ in water vapor using a tunable diode laser-based spectrometer

Jian Zhang[1] · Junya Du[1] · Cong Jiang[1] · Tianbo He[1] · Jingsong Li[1]

Received: 7 March 2023 / Accepted: 17 April 2023 / Published online: 3 May 2023

Abstract
A gas detection system based on tunable diode laser absorption spectroscopy (TDLAS) was reported, which can be used for real-time, continuity, high-precision, and rapid time response measurement of the isotope ratio of $^{18}O/^{16}O$ in water vapor from 3729.8 cm^{-1} to 3730.8 cm^{-1}. A detailed description of the system's implementation was provided and preliminary measurement precision was analyzed with a short path length sample cell (20.4 cm) after verification in the laboratory environment. Allan variance analytical method was used to evaluate the reliability of the developed laser spectroscopic isotope analysis system and the results showed that a precision of 5.274‰ was obtained for $^{18}O/^{16}O$ ratio at 1 s signal averaging time, which can be improved to 0.088‰ at the integration time of approximate 191 s. By combining with a long optical path absorption cell, the developed TDLAS isotope detection system provides great potential for determining the oxygen isotope composition of water vapor for various applications in environmental, geological, ecological, and energy fields.

1 Introduction

Water (H_2O) is a core element of the ecology and environment, and an essential component of all life on Earth. The reasonable utilization and effective protection of water resources depend largely on the level of understanding of the water cycle [1]. Stable isotope analysis is a powerful tool in modern science and has important applications in the study of geology, meteorology, and earth sciences. The analysis of isotopes in water provides an important basis for researching the formation, movement, and composition change mechanism of water, lays the foundation for the rational use of precious water resources, and plays a crucial role in probing the cycle processes of global water. Firstly, the variation of hydrogen and oxygen isotope ratios can effectively reflect the source of water and climate changes in the region [2, 3]. Secondly, water isotope ratio data can be used to analyze and explore the distribution pattern of natural precipitation isotopes [4, 5]. Finally, isotopic data can obtain a wealth of relevant information in water cycling, applied to continuously update hydrological science from multiple perspectives [6, 7]. In addition, it is possible to analyze the degree of pollution of the ocean by studying the water isotope ratios [8].

Generally, isotope ratios are measured by isotope ratio mass spectrometry (IRMS) [9], an expensive instrument that requires specialized technicians and is costly to operate and maintain [10]. The main IRMS technologies for measuring stable isotope ratios are traditional off-line dual inlet isotope ratio mass spectrometry (Dual inlet-IRMS) [11], continuous-flow isotope ratio mass spectrometry with GasBench (GasBench-IRMS) [12], thermal conversion/elemental analyzer isotope ratio mass spectrometry (TC/EA-IRMS) [13]. However, IRMS can't measure water vapor directly and requires pretreatment. Water vapor sample is usually collected by some chemical or physical method, such as isotope fractionation. Due to the complex steps and time-consuming sample pretreatment process, water isotope ratios measured by traditional IRMS techniques are easily affected by the external environment, even causing mistakes in the measurement results [10, 14].

With the rapid advancement of current laser spectroscopy techniques, real-time and high-precision isotopic monitoring in water vapor can be realized, eliminating the influence of seasons and weather [15, 16]. Typical laser spectroscopy measurement methods include integrated cavity output spectroscopy [17], cavity ring-down spectroscopy [18], tunable laser absorption spectroscopy [19], etc. For water isotope ratio measurements, the above methods have

✉ Jingsong Li
ljs0625@126.com

[1] Laser Spectroscopy and Sensing Laboratory, Anhui University, Hefei 230601, China

obvious advantages over IRMS, such as simple experimental systems, uncomplicated procedures, rapid response characteristics, in situ deployment, low operation and maintenance costs, and more importantly, direct sample measurement without complicated pretreatment. For example, Maselli et al. utilized a laser water isotope analyzer to measure the D/H and $^{18}O/^{16}O$ isotope ratio in large amounts of ice core samples for reconstructing the Paleo-environmental [20]. Gaj et al. measured the D/H and $^{18}O/^{16}O$ isotope ratio in H_2O in semi-arid areas [21]. Han et al. measured the water isotope ratios in the atmosphere, plant tissue, and soil pools [22].

Tunable diode laser absorption spectroscopy (TDLAS) is a simple gas detection method based on the well-known Lambert–Beer law. In theory, TDLAS is a calibration-free spectroscopy technique, assuming that relevant experimental conditions are known, such as temperature, pressure, and absorption optical path, as well as the related spectral parameters. Compared to other non-optical detection methods, it is not only sensitive and accurate in measuring very low concentrations of samples, but also provides high selectivity and fast time response. Additionally, it requires only minimal sample preparation and is relatively easy and inexpensive to operate [23–27]. Therefore, TDLAS-based isotope analysis has become increasingly popular in various fields. Ryuichi et al. reported the CO_2 and H_2O isotope ratio, which revealed that the meteorological phenomena could be traced [28]. Lee et al. described a system for in situ measurement of $^{18}O/^{16}O$ of water vapor in air based on TDLAS [29]. Wen et al. conducted a simultaneous measurement of the D/H and $^{18}O/^{16}O$ isotope ratio of water vapor and captured swiftly changing signals of the isotopes [30].

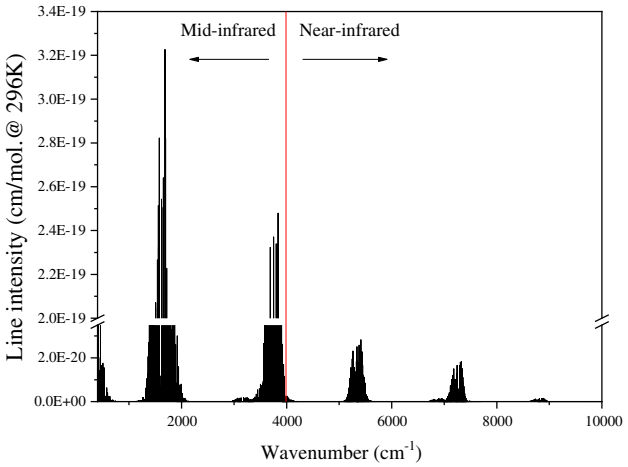

Fig. 1 Simulation of H_2O absorption lines distribution characteristics based on HITRAN database at 296 K

Figure 1 shows the simulated spectral distribution characteristics of the H_2O molecule based on the HITRAN database [31]. As can be seen, water vapor has rich absorption spectral characteristics throughout the entire infrared spectral range, especially in the mid-infrared spectral region, which corresponds to molecular fundamental transitions with strong absorption lines, making it an ideal spectral for highly sensitive gas detection and isotope analysis.

In this work, a TDLAS-based isotope ratio measurement system was developed to determine the isotopic ratio of $^{18}O/^{16}O$ in water vapor. A mid-infrared tunable diode laser with a central emitting wavelength near 2683 nm (i.e. 3727.17 cm^{-1}) was used as the excitation light source. A detailed description of the system's implementation and preliminary experimental evaluation were investigated.

2 Experimental setup

The experimental setup, as shown in Fig. 2, mainly consisted of a mid-infrared tunable diode laser, a short path optical gas cell, a detector, a gas sampling system, and a data acquisition and control system. The selected mid-infrared tunable diode laser source was purchased from Nanoplus GmbH, emitting at 3727.17 cm^{-1} with a continuous-wave distributed

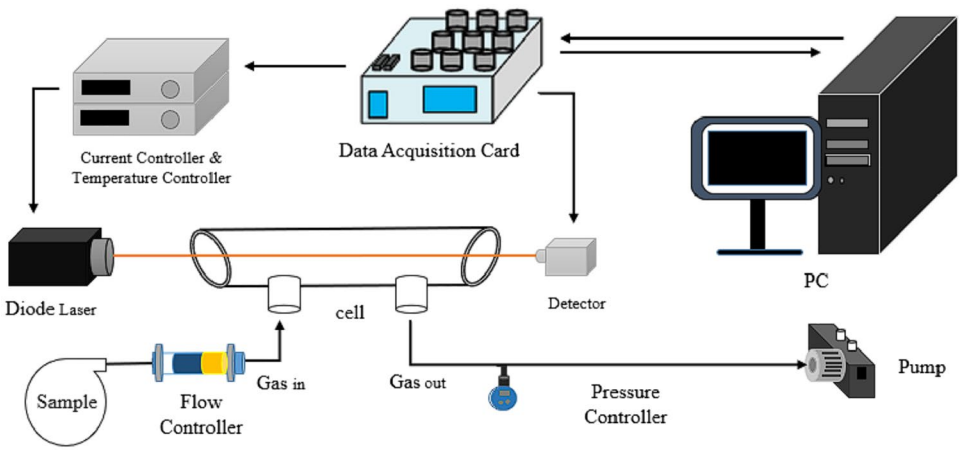

Fig. 2 TDLAS system for measuring isotope ratio of water vapor

feedback (DFB) structure. The DFB diode laser has a very high spectral purity with a line-width of less than 3 MHz, and a maximum output power of 12 mW. The laser emitting wavelength is accurately tuned by a temperature controller (TED200C, Thorlabs) and a current controller (LDC205C, Thorlabs). The laser beam was calibrated using an X–Y collimator and directly detected by a TE cooled mercury-cadmium-telluride detector (PVMI-4TE-10.6, Vigo Systems S.A.) after passing through the glass gas absorption cell with an optical length of 20.4 cm.

2.1 Laser characteristics

The laser wavelength tuning characteristics were first investigated by a high-precision wavemeter. Figure 3 shows the wavelength tuning range of the DFB diode laser at different operating temperatures (20–30 °C) and current levels (62.5–142.5 mA). The tuning coefficients of current tuning ($\Delta\nu/\Delta I$) and temperature tuning ($\Delta\nu/\Delta T$) are 0.0242 cm^{-1}/mA and − 0.319 cm^{-1}/°C, respectively. Based on these calibration lines, the measurable spectral range of the DFB diode laser is between 3726.111 cm^{-1} and 3731.266 cm^{-1}.

2.2 Gas sampling system

The gas sampling system was composed of a vacuum pump, a pressure gauge (Testo-552, Germany) and a flow meter (MCR-2000 slpm, ALICAT), and several two-way and three-way valves. Generally, H_2O molecules adhered to the walls of the absorption cell due to its high polarity, decreasing the system's response time and causing fractionation effects [29]. The residual water from experiments and the water vapor in the air also caused a memory effect in the absorption cell. Therefore, it was necessary to clean the absorption cell using dry nitrogen (N_2) several times before the experiment. Afterward, the intake valve of the water vapor sample bottle was opened to let in the water vapor. The flow rate of the gas was regulated by a flow meter to make the water vapor pass through the absorption cell uniformly and reduce the memory effect. The pressure controller was used to control the pressure in the system.

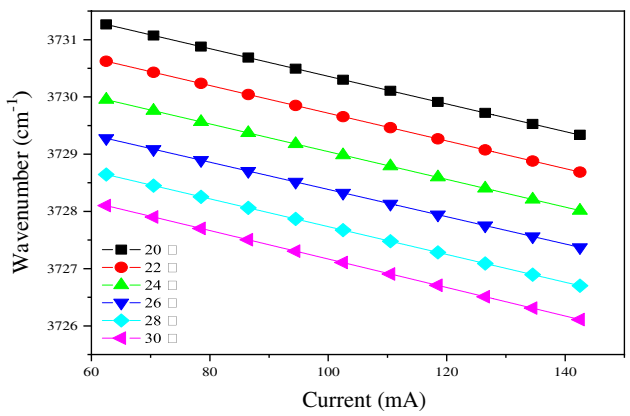

Fig. 3 The tuning of the DFB laser at different operating currents and temperatures

2.3 Data acquisition and control system

A data acquisition I/O card (NI USB-6361), and the laptop were connected using USB for driving the laser and data acquisition. A 100 Hz saw tooth tuning waveform generated from a self-developed LabVIEW program was used to scan laser over the absorption feature of H_2O isotopes. The signals were processed with a custom-made multi-peak fitting program in LabVIEW. The absorption spectrum was fitted and quantified using the H_2O molecular spectral parameters in the HITRAN database. Each spectrum was the average value of the signal obtained from 100 separate scans (corresponding to a measurement time of ~ 1 s), to increase the signal-to-noise ratio (SNR). Finally, the measured spectral data was saved for further analysis.

3 Results and discussion

3.1 Selection of absorption lines

The selection of spectral absorption lines is the most critical step in the measurement of an isotope ratio as it has a significant effect on the results and accuracy of the measurement system. Firstly, to prevent interference from any other gas present in the air, it is essential to ensure the independence of the absorption lines. Additionally, the line intensity should be appropriate for the TDLAS system to maximize the detection sensitivity.

Figure 4 (a) illustrates the simulated absorption spectrum of 1% H_2O and 400 ppm CO_2 in the range of 3729.8 cm^{-1} to 3730.8 cm^{-1}; Fig. 4 (b) displays the corresponding line intensity. Table 1 shows two absorption line parameters of $H_2{}^{16}O$ and $H_2{}^{18}O$ in this range. As shown in Table 1, these two absorption lines are suitable for isotope measurements of H_2O because they have stronger line intensities of 10^{-22} cm/molecule and have similar lower ground-state energies that minimize the effect of temperature. As can be seen from Fig. 4 (b), two CO_2 absorption lines near them. Noise and the limitation of the laser performance will make the CO_2 absorption line at 3730.4688 cm^{-1} and 3730.5146 cm^{-1} difficult to detect. Therefore, the absorption lines at 3730.4766 cm^{-1} and 3730.5579 cm^{-1} were still selected in this work.

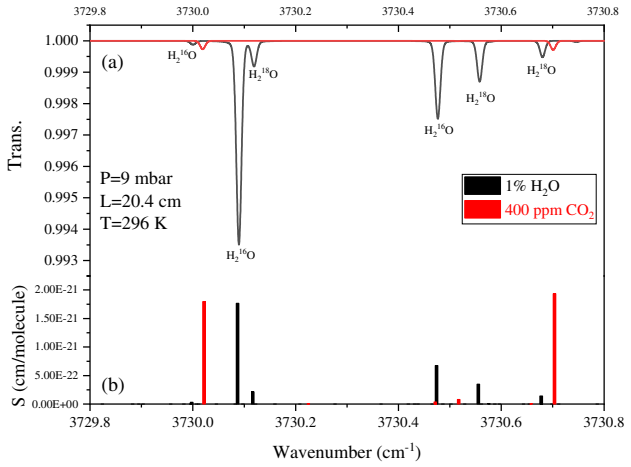

Fig. 4 **a** Shows simulations of the absorption spectrum of 1% H_2O and 400 ppm CO_2 in the range of 3729.8 cm^{-1} to 3730.8 $cm.^{-1}$ based on the HITRAN database under the conditions of a pressure of 9 mbar, an optical path of 20.4 cm, and a temperature of 296 K; **b** displays the line intensity corresponding to the absorption line. Black represents H_2O and red represents CO_2

3.2 Isotopic measurement

The isotopic ratio of an element is the ratio of minor to major isotope abundance. Since the major isotope abundance of elements in nature is usually larger than the minor isotope, the value of the isotopic ratio is small. To make practical work more convenient, a 'δ-value' is used to express the isotopic ratios. The δ-value is as follows:

$$\delta(‰) = \left(\frac{R_{\text{sample}}}{R_{\text{ref}}} - 1\right) \times 1000 \tag{1}$$

where R_{sample} and R_{ref} are the ratios of the minor to major isotopes (e.g., $^{18}O/^{16}O$) in the sample and the international reference standard known as Vienna Standard Mean Ocean Water (VSMOW), respectively. In the absorption spectrum, R_{sample} is generally determined with a ratio of absorption intensity 'S', isotope abundance 'n', and integral area 'A'. The δ-value represents the relative difference between the $^{18}O/^{16}O$ ratio of the sample and the reference standard substance per milliliter (‰). For example, R_{sample} belongs to the $^{18}O/^{16}O$ ratio:

$$R_{sample} = \frac{{}^{18}A \times {}^{18}n \times {}^{16}S}{{}^{16}A \times {}^{16}n \times {}^{18}S} \tag{2}$$

The superscripts 18 and 16 refer to molecules $H_2{}^{18}O$ and $H_2{}^{16}O$ respectively. The values of 'n' and 'S' can be obtained from the HITRAN database, and 'A' is the integral area of absorption lines of the minor and major isotopic components. The isotope abundance of $H_2{}^{16}O$ and $H_2{}^{18}O$ are 0.997317 and 1.99983‰, respectively.

This work was carried out in laboratory condition, where the temperature was controlled by the air conditioner in the lab. The current and temperature of the DFB laser are 90 mA and 21 ℃, respectively. Monitored and recorded temperature and humidity with a hygrothermograph. The saw tooth tuning waveform with an amplitude of 0.35 V and a scan frequency of 100 Hz was used to modulate the laser.

As shown in Fig. 5 (a), the 'Exp. data' is the $H_2{}^{16}O$ and $H_2{}^{18}O$ absorption lines measured in the experiment with a pressure of 9 mbar, an optical path of 20.4 cm, and a temperature of 298.4 K. The signal was collected by the self-made LabVIEW signal acquisition program, with 600 sampling points and 100 averages, and data was recorded every 1 s. In consideration of the laser intensity ramp, the 'Polynomial fitting' is the baseline obtained by polynomial fitting. Figure 5 (b) shows the transmittance function with a high

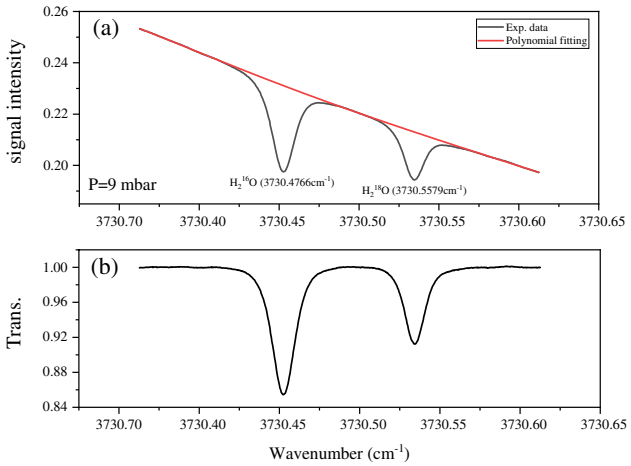

Fig. 5 **a** Shows the experimental data of water vapor from pure water under the conditions of pressure = 9 mbar, optical path = 20.4 cm, temperature = 298.4 K. The smoothing curve is the baseline obtained by the polynomial fitting; **b** shows the transmittance function

Table 1 Absorption line parameters for measuring water vapor isotope ratio (from HITRAN database, version 2020)

Isotopologue	Frequency (cm^{-1})	Line strength (cm/molecule)	Ground-State energy (cm^{-1})	Temperature coefficient at 296 K(‰, K^{-1})
$H_2{}^{16}O$	3730.4766	6.745E-22	300.4	4.6
$H_2{}^{18}O$	3730.5579	3.479E-22	282.3	1.5

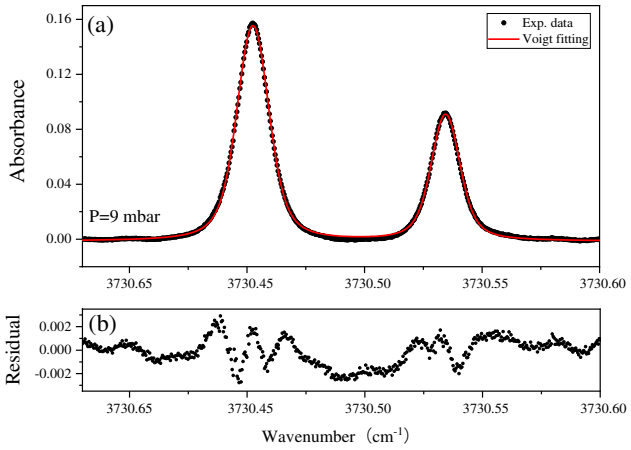

Fig. 6 **a** shows the H_2O absorbance spectrum under the experimental conditions of pressure = 9 mbar, optical path = 20.4 cm, temperature = 298.4 K. The smooth curve is the best-fitted curve with the Voigt profile function, **b** shows the corresponding fitting residuals

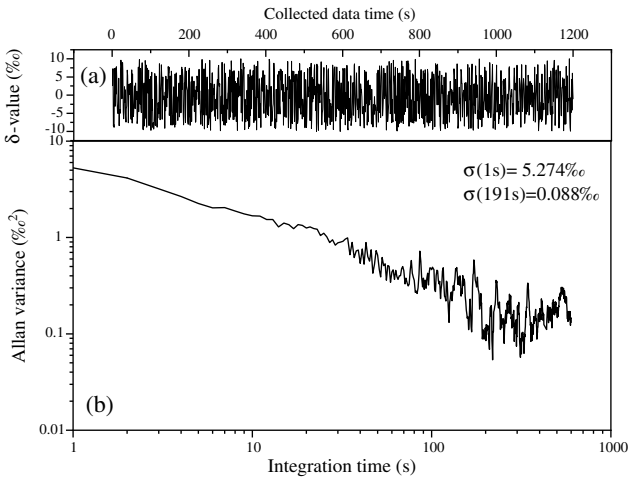

Fig. 7 **a** shows the time acquisition sequence of $\delta^{18}O$ with an interval of 1 s; **b** shows the Allan variance

SNR, which is consistent with the simulations based on the HITRAN database.

Figure 6 (a) shows the H_2O absorbance value measured in the spectral range of 3730.38 cm^{-1} to 3730.60 cm^{-1}. The fitting method of nonlinear least squares combining the Levenberg–Marquardt algorithm and Voigt profile model was used for determining the integrated area under the absorption line. Because the fitting integral area will largely determine the final measurement accuracy, the fitting residuals can be used for evaluating signal processing quality. As can be seen in Fig. 6 (b), the fitting residual of less than ± 0.003 is obtained in this work. The W-shaped fitting residuals in Fig. 6 (b) can be effectively eliminated using advanced line shape models, such as Rautian profile [32] and Galatry profile [33], which take into consideration the Dicke narrowing effect and can obtain a better fit than the Voigt profile [34]. The concentration of H_2O can be directly calculated by combining the integral area of absorption lines, pressure, optical path, and temperature. The average concentrations of $H_2{}^{16}O$ and $H_2{}^{18}O$ were 100.00% and 99.96% respectively, which were similar to the pure water sample.

The sensitivity of experimental detection results is greatly affected by the system stability. It can be improved by increasing the average times of the measurement of the spectrum. Theoretically, the detection sensitivity of a system can be improved by infinitely averaging the spectrum. However, due to some factors such as laser frequency shift, pressure variation, and thermal fluctuation, which affect the system stability, each measurement system based on laser absorption spectroscopy can only be stable for a limited time. The Allan variance can be used to determine the optimal time.

The reliability of the system was evaluated by continuous measurements over 20 min. Figure 7 (a) shows $\delta^{18}O$ values, and the average value of $\delta^{18}O$ is -0.6616‰. Time series concentrations show similar trends during measurements, which demonstrates the reliability of the developed isotope detection system; Fig. 7 (b) shows the analysis results of time series data. As shown in the Allan variance results, when the integration time is 1 s, the measurement precision of $\delta^{18}O$ is 5.274‰, and it can be enhanced to 0.088‰ with an integration time of 191 s, the best stability time of the system.

3.3 Air measurement

The developed isotope detection system was evaluated in the laboratory for evaluating the detection sensitivity of H_2O isotope ratios in air. As shown in Fig. 8 (a), the "Exp. data" is the $H_2{}^{16}O$ and $H_2{}^{18}O$ absorption lines in air measured at a pressure of 60 mbar and a temperature of 294.8 K. The two absorption lines of H_2O in Fig. 8 (a) are 3730.4766 cm^{-1} and 3730.5579 cm^{-1}, respectively. These two lines were fitted to Voigt, thus the integrated area of each absorption line was determined for isotope analysis. Figure 8 (b) is the fitting residual of the experimental spectrum, which is less than ± 0.0015. The water vapor concentration obtained after calculation was 1.125%, and the humidity measured by the hygrometer is 50.0%, which translates into a concentration of 1.143%. The error of the measured concentration is 1.26%. In contrast, the precision of isotope measurements for water vapor in the air is not ideal, which can be improved by updating the isotope detection system in future work.

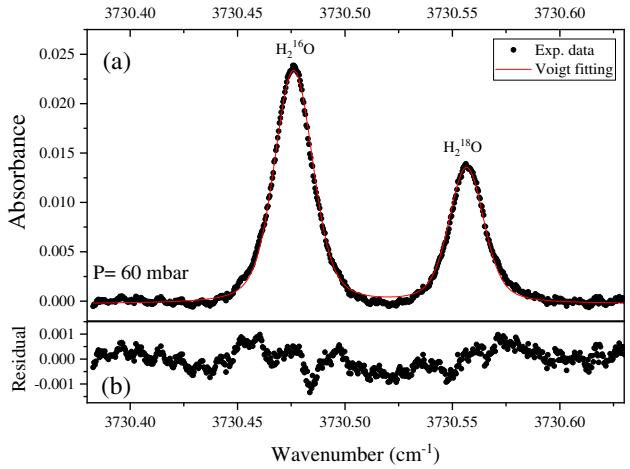

Fig. 8 **a** Shows the H_2O absorbance spectrum of indoor air under the experimental conditions of pressure = 60 mbar, H_2O mixing ratio in air = 1.143%, temperature = 294.8 K. The smooth curve is the best-fitted curve with the Voigt profile function; **b** shows the fitting residual

4 Conclusions

In conclusion, the feasibility of determining the isotope ratio in water vapor was demonstrated by the self-made measurement system. Two optimum absorption lines, $H_2{}^{16}O$ ($V_0 = 3730.47661\ cm^{-1}$) and $H_2{}^{18}O$ ($V_0 = 3730.55794\ cm^{-1}$) were selected for the measurement of the $\delta^{18}O$ values in water vapor. The reliability of the long-term measurement of the system was evaluated. The developed TDLAS isotope detection system enables real-time, continuous, high-precision, and rapid time response measurement of the isotope ratio in H_2O, providing great potential for determining oxygen isotope composition of water vapor for various applications in the environmental, geological, ecological, and energy fields. Future work will focus on improving the developed TDLAS isotope detection system to achieve higher precision measurements in a complex environment.

Acknowledgements This work was financed by the National Natural Science Foundation of China (41875158 and 61675005), the Open Fund of Key Laboratory of Opto-electronic Information Technology, Ministry of Education of Tianjin University (2022KFKT011).

Author contributions Jian Zhang: Investigation, Methodology, Data curation, Formal analysis, Visualization, Writing-original draft. Junya Du: Data curation, Software, prepared figures 1-4 and table 1. Cong Jiang: Data curation, Software, prepared figures 5-8. Jingsong Li: Conceptualization, Methodology, Investigation, Writing-review & editing, Project administration, Funding acquisition. Tianbo He: Troubleshooting, Data assessment.

Declarations

Conflict of interest The authors declare no competing interests.

References

1. G.J. Bowen, Z. Cai, R.P. Fiorella, A.L. Putman, Annu. Rev. Earth Planet. Sci. **47**, 453 (2019)
2. X. Wu, F. Chen, X. Liu, S. Wang, M. Zhang, G. Zhu, X. Zhou, J. Chen, Water **13**, 2374 (2021)
3. R. van Geldern, J. Kuhlemann, R. Schiebel, H. Taubald, J.A.C. Barth, Isot. Environ. Health Stud. **50**, 184 (2014)
4. P.R. Lekshmy, M. Midhun, R. Ramesh, J. Hydrol. **563**, 354 (2018)
5. Z. Wei, K. Yoshimura, A. Okazaki, K. Ono, W. Kim, M. Yokoi, C.T. Lai, J. Hydrol. **533**, 91 (2016)
6. J.J. Gibson, T.W.D. Edwards, S.J. Birks, N.A. St Amour, W.M. Buhay, P. McEachern, B.B. Wolfe, D.L. Peters, Hydrol. Process. **19**, 303 (2005)
7. Z. Pang, Y. Kong, J. Li, J. Tian, Proced Earth Planet. Sci **17**, 534 (2017)
8. P. Schlosser, R. Bayer, G. Bönisch, L.W. Cooper, B. Ekwurzel, W.J. Jenkins, S. Khatiwala, S. Pfirman, W.M. Smethie, Sci. Total Environ. **237–238**, 15 (1999)
9. P. Gupta, D. Noone, J. Galewsky, C. Sweeney, B.H. Vaughn, Rapid Commun. Mass Spectrom. **23**, 2534 (2009)
10. E. Kerstel, L. Gianfrani, Appl. Phys. B **92**, 439 (2008)
11. S.D. Kelly, K.D. Heaton, P. Brereton, Rapid Commun. Mass Spectrom. **15**, 1283 (2001)
12. D. Paul, G. Skrzypek, Rapid Commun. Mass Spectrom. **20**, 2033 (2006)
13. W. Meier-Augenstein, H.F. Kemp, S.M.L. Hardie, Food Chem. **133**, 1070 (2012)
14. P. Sturm, A. Knohl, Atmos. Meas. Tech **3**, 67 (2010)
15. N. Kurita, B.D. Newman, L.J. Araguas-Araguas, P. Aggarwal, Atmos. Meas. Tech. **5**, 2069 (2012)
16. F. Aemisegger, P. Sturm, P. Graf, H. Sodemann, S. Pfahl, A. Knohl, H. Wernli, Atmos. Meas. Tech. **5**, 1491 (2012)
17. M.F. Nehemy, C. Millar, K. Janzen, M. Gaj, D.L. Pratt, C.P. Laroque, J.J. McDonnell, Rapid Commun. Mass Spectrom. **33**, 1301 (2019)
18. J. Liu, C. Xiao, M. Ding, J. Ren, J. Environ. Sci. **26**, 2266 (2014)
19. C.R. Pidgeon, M.J. Colles, Nature **279**, 377 (1979)
20. O.J. Maselli, D. Fritzsche, L. Layman, J.R. McConnell, H. Meyer, Isot. Environ. Health Stud. **49**, 387 (2013)
21. M. Gaj, M. Beyer, P. Koeniger, H. Wanke, J. Hamutoko, T. Himmelsbach, Hydrol. Earth Syst. Sci. **20**, 715 (2016)
22. J. Han, L. Tian, Z. Cai, W. Ren, W. Liu, J. Li, J. Tai, J. Hydrol. **608**, 127672 (2022)
23. S. Lin, J. Chang, J. Sun, P. Xu, Front. Phys. (2022). https://doi.org/10.3389/fphy.2022.853966
24. C. Jiang, J. Zhang, Z. Xi, W. Ma, J. Li, Spectrochim. Acta Mol. Biomol. Spectrosc. **281**, 121628 (2022)
25. F. Xin, J. Li, J. Guo, D. Yang, Y. Wang, Q. Tang, Z. Liu, Sensors **21**, 1722 (2021)
26. G. Durry, J.S. Li, I. Vinogradov, A. Titov, L. Joly, J. Cousin, T. Decarpenterie, N. Amarouche, X. Liu, B. Parvitte, O. Korablev, M. Gerasimov, V. Zéninari, Appl. Phys. B **99**, 339 (2010)
27. P. Werle, R. Macke, F. Slemr, Appl Phys B Photophys Laser Chem **57**, 131 (1993)
28. R. Wada, Y. Matsumi, T. Nakayama, T. Hiyama, Y. Fujiyoshi, N. Kurita, K. Muramoto, S. Takanashi, N. Kodama, Y. Takahashi, Isot. Environ. Health Stud. **53**, 646 (2017)
29. X. Lee, S. Sargent, R. Smith, B. Tanner, J. Atmos. Oceanic Tech. **22**, 555 (2005)
30. X.-F. Wen, X.-M. Sun, S.-C. Zhang, G.-R. Yu, S.D. Sargent, X. Lee, J. Hydrol. **349**, 489 (2008)
31. I.E. Gordon, L.S. Rothman, R.J. Hargreaves, R. Hashemi, E.V. Karlovets, F.M. Skinner, E.K. Conway, C. Hill, R.V. Kochanov, Y. Tan, P. Wcisło, A.A. Finenko, K. Nelson, P.F. Bernath, M. Birk, V.

Boudon, A. Campargue, K.V. Chance, A. Coustenis, B.J. Drouin, J. Quant. Spectrosc. Radiat. Transfer **277**, 107949 (2022)
32. L. Galatry, Phys. Rev. **122**, 1218 (1961)
33. J.S. Li, G. Durry, J. Cousin, L. Joly, B. Parvitte, V. Zeninari, J. Quant. Spectrosc. Radiat. Transfer **111**, 2332 (2010)
34. C.-M. Chou, R.-Y. Wang, Hydrol. Process. **18**, 987 (2004)